eters were calibrated with the melting point of ice and boiling point of distilled water. Each observation was taken after running the still for at least 3 h.

Analyses. The standard succinic acid solution was prepared by weighing solid succinic acid accurately and dissolving it in a known volume of distilled water. The sodium hydroxide solution was standardized by using standard succinic acid solution with phenolphthalein as indicator. Weight percent acetic acid in aqueous solution in vapor phase was estimated by titrating a known amount of solution against standardized sodium hydroxide solution with phenolphthalein as indicator. Weight percent acetic acid in the aqueous solution in the liquid phase was determined by material balance. The results were reproducible with a maximum error of 0.1%.

Results and Discussion

Table I contains the experimental vapor-liquid equilibrium data for water (1)-acetic acid (2) solution without salt. Tables II-IV report the experimental data with the three salts at different salt concentrations. Tables V-VIII show the solubilities of the salts. Equilibrium curves at salt saturation are shown in Figure 1. The points in the figure are smoothed data points.

Addition of KCl, Na_2SO_4, and K_2SO_4 results in "salting out" of acetic acid. Water-acetic acid solutions containing salts KCl and Na_2SO_4 above 80 and 91 wt % water on salt-free basis, respectively, form azeotropes. An equation of the type log $(Y_s/Y_{so}) = KW$ fits the data for the three salts studied in this system. Such an equation was proposed by Yoshida et al. (*4*) for the salts NaCl, $MgCl_2$, $NaNO_3$, Na_2SO_4, and $CaCl_2$. The constants obtained are KCl, $K = 8.2 \times 10^{-3}$; Na_2SO_4, 13.0×10^{-3}; K_2SO_4, 8.0×10^{-3}.

The thermodynamic consistency was assessed by applying Herrington's criteria (*7*, *8*). Herington's isobaric consistency test is not very accurate for aqueous systems. The absolute value of $(D - J)$ to be less than 10 is good for systems having the ratio of the maximum value of heat of mixing to the maximum value of excees free energy of mixing, greater than or equal to three.

The values of D and J are

	D	J
without salt	12.3	7.1
saturated with KCl	2.7	15.7
saturated with Na_2SO_4	36.4	25.7
saturated with K_2SO_4	28.3	24.0

Glossary

D	percent deviation, $100\ I/\Sigma$
I	difference between the area above and below the abscissa when log (γ_1/γ_2) is plotted against x_i
J	$150\theta/T_{min}$
K	proportionality factor
T_{min}	lowest boiling point in the system, K
W	weight percent of salt in liquid solution on salt-free basis
x_i	mole fraction of component i in liquid phase on salt-free basis
y_i	mole fraction of component i in vapor phase
Y_s	mole fraction of organic solvent in vapor phase in salt solution
Y_{so}	mole fraction of organic solvent in vapor phase in salt-free (without salt) solution

Greek letters

θ	difference in temperature between maximum and minimum boiling point, K
Σ	total integral area

Subscripts

1	water
2	acetic acid

Registry No. KCl, 7447-40-7; Na_2SO_4, 7757-82-6; K_2SO_4, 7778-80-5; acetic acid, 64-19-7.

Literature Cited

(1) Johnson, A. I.; Furter, W. F. *Can. J. Chem. Eng.* **1960**, *38*, 78-87.
(2) Nishi, Y. *Chem. Eng. Jpn.* **1975**, *8*, 187-191.
(3) Tursi, R. R.; Thompson, A. R. *Chem. Eng. Prog.* **1951**, *47*, 304-308.
(4) Yoshida, F.; Yasunishi, A.; Hamada, Y. *Kagaku Kogaku* **1964**, *2*, 162-166.
(5) Bedrossian, A. A.; Cheh, H. Y. *AIChE Symp. Ser.* **1974**, *70*, 102-109.
(6) Jaques, D. *Can. J. Chem. Eng.* **1975**, *53*, 713-715.
(7) Jaques, D.; Furter, W. F. *AIChE J.* **1972**, *18*, 343-346.
(8) Herington, E. F. G. *J. Inst. Pet.* **1951**, *37*, 457-460.

Received for review March 20, 1984. Revised manuscript received March 25, 1985. Accepted May 13, 1985.

Equilibrium Phase Compositions, Phase Densities, and Interfacial Tensions for CO_2 + Hydrocarbon Systems. 1. CO_2 + *n*-Butane

Jack J.-C. Hsu, N. Nagarajan, and R. L. Robinson, Jr.*
School of Chemical Engineering, Oklahoma State University, Stillwater, Oklahoma 74078

An experimental facility has been established for measurements of equilibrium phase compositions, phase densities, and interfacial tensions in mixtures of interest in petroleum reservoir engineering. Data have been obtained on the system CO_2 + *n*-butane at 115, 160, and 220 °F at pressures to the critical point (interfacial tensions as low as 0.03 mN/m). The measured phase compositions and densities agree well with the work by Sage and Lacey. The interfacial tension data are in reasonable agreement with the measurements of Stegemeier (115 and 160 °F), with the present results extending to lower values of interfacial tension.

Introduction

The development of efficient, economical methods for secondary or tertiary recovery of petroleum reservoir fluids could substantially increase our nation's usable reserves and supply of energy. The use of carbon dioxide (CO_2) for the miscible displacement of petroleum is one such recovery method. The CO_2 flooding technique has proved sufficiently promising that it is currently under intensive laboratory and field study. However, the mechanisms by which CO_2 floods operate are not fully understood.

Evidence exists that so-called "miscible" displacements of oil by CO_2 actually operate, in substantial part, in the immiscible

0021-9568/85/1730-0485$01.50/0

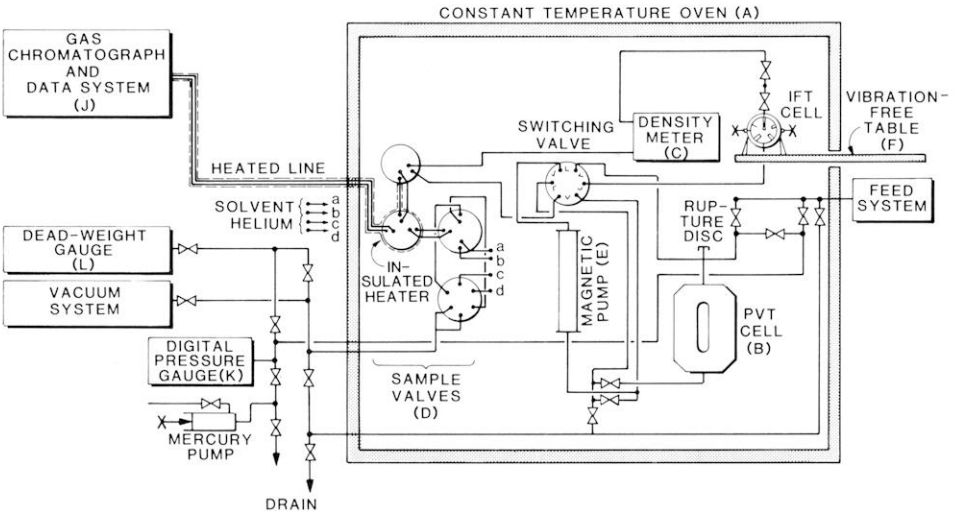

Figure 1. Apparatus for measurement of equilibrium phase compositions, densities, and interfacial tensions.

or "near" miscible regimes. These regimes occur in several circumstances, including (a) displacements which operate below but near the CO_2 minimum miscibility pressure, (b) situations where multiple liquid phases are formed by the CO_2–oil mixtures, and (c) when the injected CO_2 slug is degraded by mixing effects during the displacement. The mechanisms of the immiscible displacements are not as well understood as those for miscible displacements. In immiscible displacements, the efficiency of the recovery process can be affected by the interfacial tension (IFT) between the fluid phases present in the reservoir. The displacement efficiency of the driving fluid depends on the IFT through the effect that IFT exerts on the capillary pressure gradient in the reservoir and on the relative permeabilities of the flowing phases. Existing data show that, at sufficiently low IFT values, displacement efficiencies under immiscible conditions can approach those for miscible floods. These improved efficiencies occur only at very low values of IFT. Studies (see, e.g., ref *1* and *2*) have demonstrated that the IFT's must certainly be less than 0.1 mN/m (0.1 dyn/cm) and perhaps as low as 10^{-3} mN/m.

If the effects of IFT on recoveries from CO_2 flooding are to be incorporated into computer simulations of the displacement process, models must be developed to predict the IFT behavior of CO_2 + hydrocarbon systems. Furthermore, such correlations must be accurate at very low values of IFT. However, experimental data on such systems are scarce (*3*, *4*); thus, correlation testing and development have been hampered.

The goal of our present research is to obtain fundamental data on interfacial tensions in CO_2–hydrocarbon systems to serve as the basis for better understanding of the effects of temperature, pressure, and composition on the IFT in such systems. These data could also lead to improved understanding of the process of miscible (or near-miscible, low-IFT) displacement of reservoir oils by CO_2 injection.

Experimental Facility

The experimental facility is illustrated schematically in Figure 1. The arrangement shown is designed so that a single charge of fluid may be employed for all property measurements (phase compositions, phase densities, and IFT). In the following description of the apparatus, letters in parentheses refer to entries in Table I, which lists the specific suppliers and model numbers of the various components used in the apparatus. Where appropriate, these letters are also used to identify parts in Figure 1.

Parts of the apparatus that require precise temperature control are housed in a commercial air oven (A). These parts include a high-pressure see-through windowed PVT cell (B), the vibrating U-tube portion of a digital density meter (C), an IFT cell, switching and sampling valves (D), and a magnetic recirculation pump (E). The magnetic pump may be operated to recirculate either liquid or vapor through the sampling valves, the U-tube of density meter, and the IFT cell. The six-port switching valve, besides facilitating selection of either vapor or liquid circulation, reverses the direction of circulation in the density cell when changing from liquid to vapor circulation. Upward flow through the cell is used for liquid circulation and downward flow for vapor. This operation gives effective displacement of the liquid from the U-tube of the density meter when circulation is switched from liquid to vapor.

The IFT cell is identical in design with that used by Jennings (*5*) and was machined by Temco, Inc., of Tulsa. The cell employs the pendant drop technique to measure IFT's. Inside the cell, several needles of outer diameters ranging from 0.0285 in. (0.725 mm) to 0.005 in. (0.125 mm) are mounted on a rotating turret. This set of needles permits measurement of IFT's in the range from approximately 20 to 0.01 mN/m (or

Table I. Sources of Equipment for the Phase Equilibrium and Interfacial Tension Facility

A : Hotpack Corporation air oven: Model 2120512 Supermatic oven
B: Ruska see-through windowed *PVT* cell: Model 2329-800-00; 10 000 psi at 300 °F
C: Mettler/Paar digital density meter: Model DMA 60, DMA 512; 6000 psi at 150 °C
D: Valco switching and sampling valves: Models AH-6-FSV-4-UHTa-H60, AH-6-V-6-UHTa-N60, AH-6-V-8-HTa, AH-6-V-6-HTa, 3000 psi at 300 °C
E: Ruska magnetic circulating pump: Model 2330-800-00; 12 000 psi at 350 °F
F: Technical Manufacturing Corporation desk style Micro-g vibration isolation table
G: Wild zoom stereo microscope: Model M7A; Model MPS45 Photoautomat exposure controller
H: "VOLPI" fiber optic light source 10-2062
I: Vanguard Instrument Corporation: Model C-110 motion analyzer
J: Varian Gas Chromatograph: Model 3700 Data System Model CDS-111
K: Heise digital pressure indicator: Model 710 A; 0–3000 psi
L: Ruska gas lubricated piston pressure gauge: Model 2470; 0–2500 psi
M: GCA Precision Scientific Co. "Thermotrol" temperature controller: Model 1053A
N: Minco resistance thermometer bridge: Model RT3 8078; thermometer Model S7929P180C
O: DORIC digital temperature indicator (Trendicator): Model 412 A

dyn/cm), corresponding to drop sizes ranging from 2.0 to 0.15 mm in diameter. The rotating turret allows a proper sized needle to be rotated into the vertical operating position without interrupting the continuity of the experiment. A secure seal between the rotating needles and a liquid delivery port (drilled in the top of the cell body) is provided by Teflon packing and an O ring between each needle and the cell wall. The published cell design (*5*) was modified to permit an adjustable compressive force to be applied to the packing for each needle (by tightening a packing nut). With this modified seal, drops can be held at the tip of a needle for indefinite periods of time.

The IFT cell is mounted separately from the remainder of the apparatus in the air bath; it rests on an extension arm from a vibration-damping table (F). The extension arm passes through the wall of the air oven but is not in contact with any part of the oven.

An optical/photographic system (not shown in Figure 1) is used to photograph the pendant drops. It consists of a "Wild" M7A Stereo-Zoom microscope with attendant photographic equipment (G) and a fiber-optic light source (H). Photographs of the pendant drops are recorded on Polaroid negative-type film, then further enlarged and analyzed on a commercial image analyzer (I). Total magnifications as high as 90X are thus possible.

The phase densities are measured by using a Mettler/Parr digital density meter (C). Measurements are made by circulating saturated vapor and liquid, in sequence, through the vibrating U-tube of the density meter.

Compositional analyses of vapor and liquid samples are performed on a commercial temperature-programmed gas chromatograph (GC) and data system (J). The sampling system consists of a combination of sampling and switching valves and is capable of delivering microliter-size samples directly from the *PVT* cell to the chromatograph. The valving arrangement also permits clean-up of the valves with gas or solvent without contaminating the fluids under study.

The chromatograph arrangement, designed for separations of CO_2 and hydrocarbons from C_1 through C_{14}, employs columns of OV-101 (4 ft), Dexil 300 (2 ft), and Poropak N (2 ft). Separation of the light hydrocarbons (including CO_2) from the heavier hydrocarbons occurs on the OV-101 column. The Dexil 300 column then separates the heavier hydrocarbons. The lighter hydrocarbons and carbon dioxide are separated by the Poropak N. All analyses are done with a thermal conductivity detector. For CO_2 + *n*-butane only the Poropak N column was required.

System pressures are measured on a digital pressure gauge (K) which is calibrated periodically against a dead-weight gauge (L). Temperature in the oven is regulated by a commercial temperature controller (M) and is measured by a platinum resistance thermometer with digital readout (N). The temperatures of the various components in the oven are monitored by thermocouples and a digital temperature indicator (O).

The experimental procedure is as follows. The fluids to be studied are charged volumetrically to the apparatus; liquid solvents are degassed by evacuating their storage vessel. Sufficient fluid is injected to give the desired pressure. The magnetic pump is then operated until equilibrium is reached, as indicated by constant phase density readings. Equilibrium times range from approximately 2 h at lower pressures to 5 or 6 h near the critical pressure.

When equilibrium is established, densities of the equilibrium phases are measured, and samples are injected into the GC by actuating the automatic sampling cycle. Three or four samples are taken in sequence to check for consistency of sample analyses. The magnetic pump is then stopped and a small quantity of liquid is trapped above the delivery port to the IFT cell. A controlled amount of this trapped liquid is forced through the needle (by a regulating valve) to make a pendant drop. The drop is photographed for the profile measurements. Three or four pictures are taken of each of at least two different drops. This procedure is repeated at a series of pressures. Switching of the needles in the IFT cell is required to cover the entire IFT range; when this is done, overlapping measurements (with adjacent needle sizes) are made to evaluate the consistency of measurements on different needles. Values of $\gamma/\Delta\rho$ are calculated from the photographic images by standard techniques (*6*).

Table II. Equilibrium Phase Properties of Pure *n*-Butane[a]

temp, °F	vapor press., psia	phase densities, (kg/m) × 10^{-3} liquid	phase densities, (kg/m) × 10^{-3} vapor	interfacial tension, mN/m
115	65	0.5472	0.0119	9.57
	(65.0)	(0.5475)	(0.0110)	(9.58)
160	121	0.5127	0.0215	6.87
	(120.6)	(0.5121)	(0.0204)	(6.88)
220	241	0.4587	0.0438	3.49
	(241.2)	(0.4581)	(0.0430)	(3.48)

[a] Values in parentheses are from the literature. Vapor pressures and phase densities are by Sage and Lacey (*7*); values at 115 °F are interpolated. Interfacial tensions are by Stegemeier (*8*).

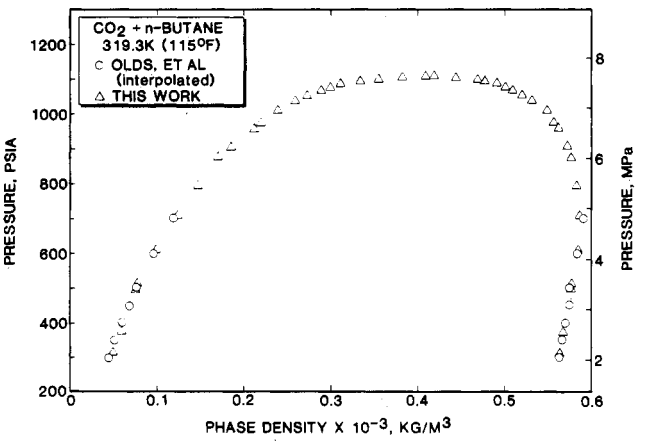

Figure 2. Comparison of phase densities at 115 °F.

Materials

The CO_2 used in these studies was supplied by Union Carbide Linde Division and had a stated purity of 99.99%. The *n*-butane was from Phillips Petroleum Co. with a stated purity of 99.98%. The chemicals were used without further purification.

Results

The complete data from the measurements for CO_2 + *n*-butane are catalogued in Tables II–IV. In the course of the measurements, the properties of pure *n*-butane have been determined. These data appear in Table II where they are compared to measurements by Sage and Lacey (*7*) and Stegemeier (*8*). For the phase densities, agreement with the data of Sage and Lacey is adequate. We assess our uncertainties in density measurements to be approximately 0.5 kg/m^3 (0.0005 g/cm^3). For interfacial tensions, agreement with the results of Stegemeier is excellent, well within our estimated experimental uncertainties of about 3% at this level of IFT. (A more detailed analysis of experimental errors is given below.) These measurements are considered adequate verification that the densitometer and IFT cell operate properly and provide reliable data.

Phase densities measured for CO_2 + *n*-butane are presented in Table III and Figures 2–4; also shown are the data of Olds et al. (*9*). At 115 °F (Figure 2), agreement is very good for

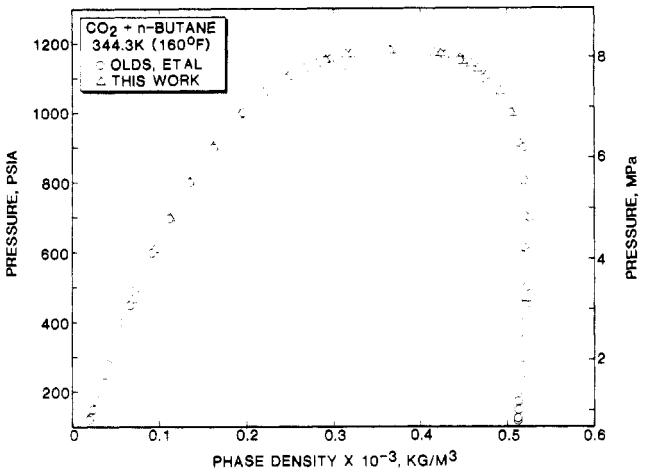

Figure 3. Comparison of phase densities at 160 °F.

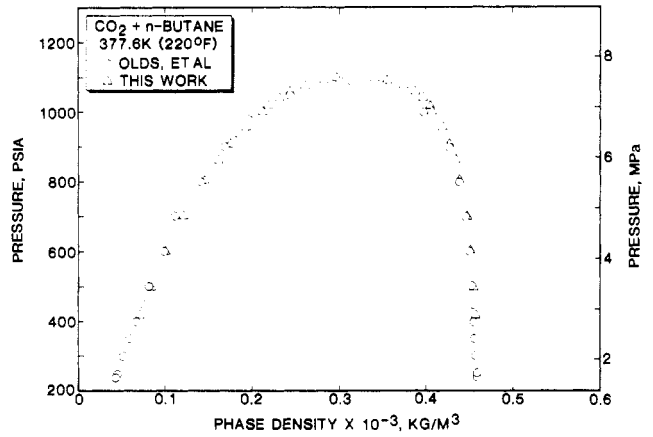

Figure 4. Comparison of phase densities at 220 °F.

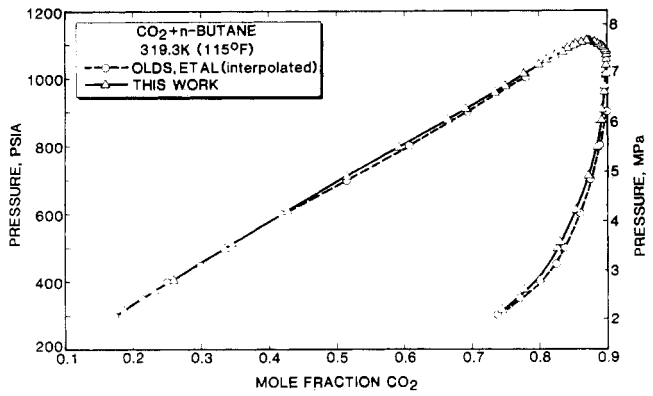

Figure 5. Comparison of phase compositions at 115 °F.

densities from this work and interpolated values from Olds et al.; no comparisons are shown above 700 psia because interpolations of the Olds et al. data become too uncertain as the critical pressure is approached. At 160 and 220 °F (Figures 3 and 4), agreement is reasonable. However, as the critical pressure is approached, the liquid densities from the present work are consistently higher than those of Olds et al.

Phase composition data are shown in Figures 5–7. Again, qualitative agreement is seen with the work of Olds et al. At 115 °F, data from the present work show somewhat lower CO_2 concentrations in both phases. At 160 and 220 °F, the reverse is true. Differences in compositions between the two data sets are typically 0.005–0.008 in mole fraction in either phase. Uncertainties in compositions from the present work are estimated to be 0.002 in mole fraction; thus, the observed differences in the two data sets are probably somewhat greater than

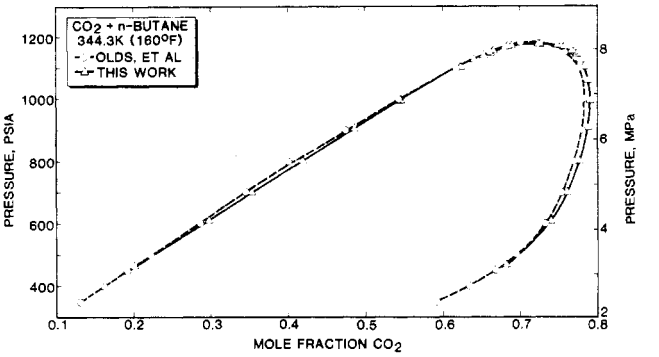

Figure 6. Comparison of phase compositions at 160 °F.

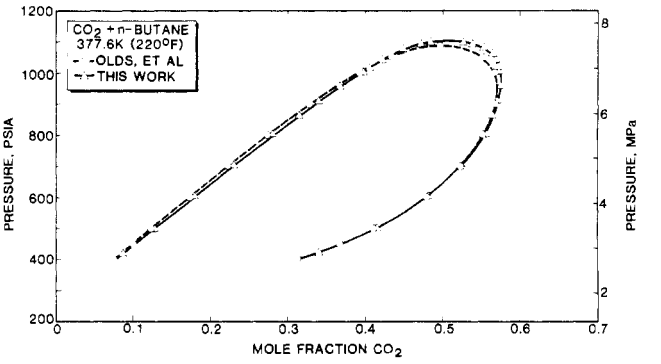

Figure 7. Comparison of phase compositions at 220 °F.

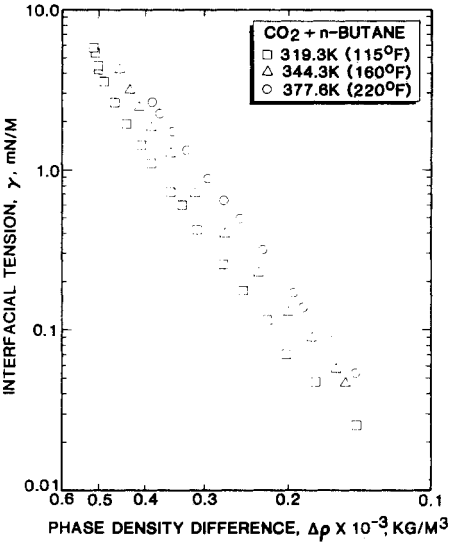

Figure 8. Relation of interfacial tension to phase density difference.

the combined estimated experimental uncertainties in the two works.

The IFT data for all three isotherms from the present work appear in Figure 8, plotted as functions of the phase density difference. This method of presenting the data conveniently expands the near-critical, low-IFT region, and "scaling laws" require that the data become linear (log–log) near the critical point.

Data are available from Brauer and Hough (*3*, *10*) for IFT values at 115 and 160 °F. Data comparisons appear in Figures 9 and 10. The comparisons are done in terms of $\gamma/\Delta\rho$ because this ratio comes directly from the measurements made on the pendant drops. Brauer did not measure $\Delta\rho$ values, but used literature data to convert $\gamma/\Delta\rho$ to γ. Thus, the $\gamma/\Delta\rho$ values provide a direct comparison of the pendant drop results of this and Brauer's works. Figure 9 shows that the two data sets agree within their experimental uncertainties at 115 °F.

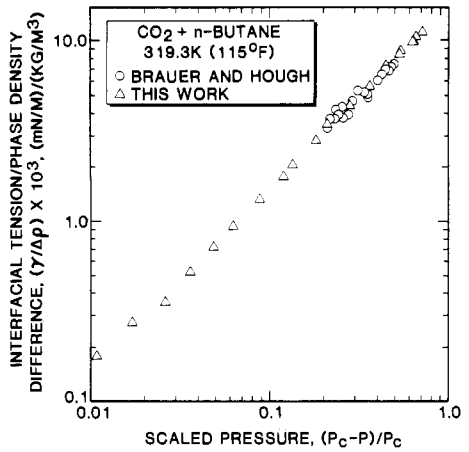

Figure 9. Comparison of interfacial tension data at 115 °F.

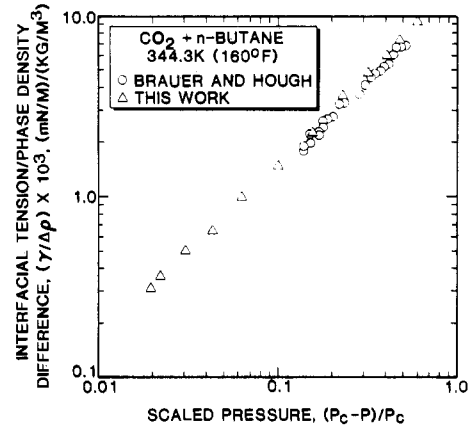

Figure 10. Comparison of interfacial tension data at 160 °F.

(Note: the data in Figure 9 are raw data from Brauer's thesis (*3*); in their publication (*10*), Brauer and Hough present only smoothed data, including points extrapolated to lower IFT's than their measurements.) At 160 °F (Figure 10), some overlap of the data sets is evident, but the present data are generally approximately 10% higher than Brauer's. On both isotherms the present data extend to lower IFT's than the work of Brauer.

In the present work, sufficient data were taken to permit an analysis of expected uncertainties in the IFT data. Multiple "readings" of IFT from each photograph were made and multiple photographs were read at each pressure–temperature point. These data facilitated the calculation of maximum deviations from the mean value of IFT for each IFT data point. The results appear in Figure 11. As expected, these estimates of uncertainties show a great deal of scatter; nevertheless, they appear to be represented reasonably well by the relationship

$$\epsilon_\gamma = 0.04\gamma^{0.8} \quad (1)$$

Equation 1 predicts maximum expected errors of 3% at γ = 10, 4% at γ = 1, 6% at γ = 0.1, and 10% at γ = 0.01 mN/m. For other properties, maximum expected uncertainties are estimated as

$$\epsilon_\rho = 0.0005 \text{ g/cm}^3 \quad (2)$$

$$\epsilon_p = 2 \text{ psi} \quad (3)$$

$$\epsilon_y = \epsilon_x = 0.002 \quad (4)$$

Average errors in these variables might be expected to be about one-half the values shown in eq 1–4.

In Table IV, estimated values of the critical-point pressure, composition, and density are given as the last entry at each temperature. Comparisons of the critical point properties of this work and of Olds et al. appear in Table IV. The critical-point

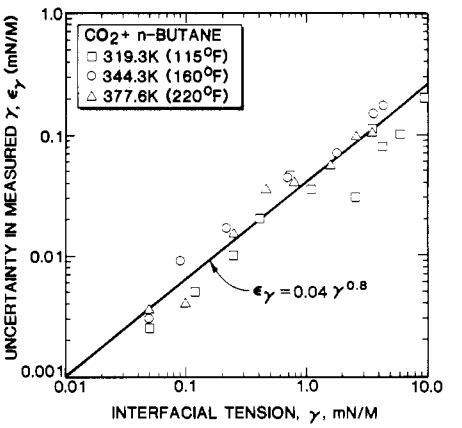

Figure 11. Maximum expected uncertainties in measured interfacial tensions.

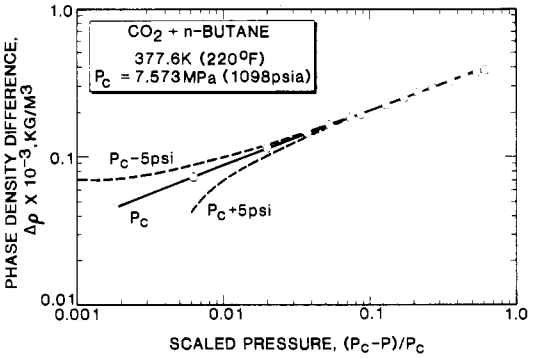

Figure 12. Effect of critical pressure on scaling-law analysis of phase density data.

densities were estimated by "rectilinear diameter" plots of $(\rho^V + \rho^L)/2$ vs. $(P_c - P)$ and critical compositions from plots $(x + y)/2$ vs. $(P_c - P)$. The critical pressure was evaluated from scaling law analyses of $\Delta\rho$ vs. P and $\gamma/\Delta\rho$ vs. P data at pressures within 10% of the critical pressure, using the following asymptotic forms of the scaling-law relations:

$$\Delta\rho = A_1[(P_c - P)/P_c]^\beta \quad (5)$$

$$\gamma/\Delta\rho = A_2[(P_c - P)/P_c]^{2\nu-\beta} \quad (6)$$

The parameters A_1, A_2, and P_c were determined by least-squares techniques; the method is illustrated in Figure 12, which shows how sensitive the linearity of the (log–log) $\Delta\rho$ vs. P relationship (eq 5) is to the value of P_c. The regressed parameters for the three isotherms included three A_1's (eq 5), three A_2's (eq 6), and three P_c's. The resultant P_c's are those given for the critical pressures in Tables III and IV. These estimates of P_c are in close agreement with visual observations; they are believed to be more reliable than the visual determinations.

In the regressions, the critical indices (β and ν) were fixed at the experimentally based values of 0.355 and 0.63 recommended by Levelt Sengers et al. (*11*). In all cases, complete weighting was employed, using eq 1–3 for the uncertainties in the measured variables. For all data points (except $\gamma/\Delta\rho$ at 115 °F, 1078 psia), the regressed values showed deviations less than the maximum expected error (based on the theory error propagation). The fit of eq 5 and 6 to the present data was marginally worse if theoretically based values of β and ν (0.325 and 0.63) were used (*12*). If β and ν were determined as part of the regression, values of 0.359 and 0.66 were obtained.

The above analysis also pointed out a suspect data point at 115 °F. This data point is very near the critical pressure and

Table III. Phase Equilibria and Interfacial Tensions for Carbon Dioxide + *n*-Butane

pressure		phase compositions, mole fraction CO_2		phase densities, $(kg/m^3) \times 10^{-3}$		interfacial tension,
kPa	psia	liquid	vapor	liquid	vapor	mN/m
			319.3 K (115 °F)			
2180	316	0.188	0.745	0.5634	0.0501	5.75
2585	375	0.232	0.778	0.5677	0.0592	5.37
3425	497	0.335	0.826	0.5767	0.0760	4.41
3545	514	0.346	0.830	0.5779	0.0779	4.27
4205	610	0.428	0.856	0.5849	0.0992	3.55
4895	710	0.515	0.873	0.5869	0.1244	2.63
5475	794	0.592	0.885	0.5835	0.1472	1.93
6035	875	0.665	0.893	0.5767	0.1713	1.42
6245	906	0.692	0.893	0.5731	0.1858	1.10
6605	958	0.735	0.896	0.5629	0.2114	0.729
6720	975	0.750	0.898	0.5573	0.2204	0.598
6965	1010	0.778	0.898	0.5495	0.2393	0.412
7155	1038	0.800	0.899	0.5320	0.2596	0.255
7260	1053	0.811	0.898	0.5212	0.2732	0.177
7355	1067	0.824	0.897	0.5103	0.2891	0.116
7435	1078	0.835	0.896	0.5015	0.3002	0.071
7500	1088	0.842	0.893	0.4919	0.3175	0.048
7550	1095	0.850	0.893	0.4782	0.3349	0.026
7585	1100	0.855	0.888	0.4700	0.3559	
7620	1105	0.864	0.882	0.4450	0.3835	
7640[a]	1108	0.873	0.876	0.4194	0.4101	
7625[b]	1106	0.875		0.4060		
			344.3 K (160 °F)			
3205	465	0.208	0.682	0.5201	0.0691	4.22
4205	610	0.297	0.740	0.5233	0.0946	3.16
4820	699	0.353	0.761	0.5229	0.1132	2.48
5530	802	0.418	0.777	0.5209	0.1352	1.85
6245	906	0.486	0.788	0.5159	0.1637	1.28
6860	995	0.545	0.791	0.5061	0.1932	0.703
7300	1059	0.590	0.788	0.4926	0.2216	0.397
7610	1104	0.623	0.783	0.4783	0.2487	0.226
7770	1127	0.641	0.778	0.4670	0.2674	0.129
7865	1142	0.653	0.773	0.4595	0.2814	0.090
7945	1152	0.663	0.768	0.4493	0.2922	0.057
7965	1155	0.666	0.767	0.4473	0.2965	0.047
8055	1168	0.682	0.757	0.4290	0.3159	
8065	1170	0.685	0.755	0.4249	0.3192	
8080	1173	0.691	0.750	0.4170	0.3284	
8120[b]	1178	0.720		0.3735		
			377.6 K (220 °F)			
2880	418	0.088	0.340	0.4565	0.0714	2.67
3435	498	0.129	0.414	0.4552	0.0836	2.24
4165	604	0.181	0.481	0.4521	0.1025	1.73
4840	702	0.230	0.525	0.4474	0.1218	1.33
5545	804	0.284	0.556	0.4399	0.1460	0.887
5950	863	0.315	0.565	0.4340	0.1617	0.646
6265	909	0.341	0.571	0.4274	0.1761	0.496
6600	957	0.368	0.575	0.4187	0.1928	0.316
6915	1003	0.398	0.573	0.4072	0.2125	0.170
7020	1018	0.406	0.572	0.4044	0.2186	0.138
7175	1041	0.423	0.569	0.3961	0.2313	0.096
7295	1058	0.434	0.565	0.3877	0.2436	0.054
7425	1077	0.452	0.554	0.3745	0.2604	
7530	1092	0.473	0.539	0.3551	0.2824	
7565	1097	0.485	0.527	0.3415	0.2967	
7580[b]	1098	0.510		0.3195		

[a] Suspect data point. [b] Estimated critical point.

Table IV. Critical Properties for CO_2 + *n*-Butane[a]

temp, °F	press., psia	density, $(kg/m^3) \times 10^{-3}$	composition, mole fraction CO_2
115	1106	0.4060	0.875
160	1178	0.3735	0.720
	(1184)	(0.3780)	(0.713)
220	1098	0.3195	0.510
	(1090)	(0.3135)	(0.498)

[a] Values in parentheses are from Olds et al. (*9*). (No values are listed at 115 °F because interpolations are too uncertain.)

is the least certain of the measured data due to the rapid changes in the phase densities as the critical pressure is approached (Figures 2–4). The suspect data point is retained in Table III, but is noted as suspect.

Conclusions

New data are presented for equilibrium phase compositions, phase densities, and interfacial tensions of CO_2 + *n*-butane at 115, 160, and 220 °F. Agreement with previous measure-

ments is adequate in regions common to both data sets. The new data present a more thorough analysis of the near-critical region; within 10% of the critical pressure, the data follow asymptotic forms of the scaling relations (eq 2 and 3).

Acknowledgment

Special thanks goes to Dr. Del D. Fussell who orginally interested us in the study of interfacial tensions.

Glossary

A_1, A_2	parameters in eq 5 and 6
P	pressure
P_c	critical pressure
x	liquid-phase mole fraction
y	vapor-phase mole fraction
β, ν	scaling-law parameters (critical indices)
γ	interfacial tension
ϵ_γ	uncertainty in measured interfacial tension
ρ^L	liquid-phase density
ρ^V	vapor-phase density
$\Delta\rho$	liquid-phase density minus vapor-phase density

Literature Cited

(1) Wagner, O. R.; Leach, R. O. *Soc. Pet. Eng. J.* **1966**, *6*, 335.
(2) Bardon, C.; Longeron, D. G. *Soc. Pet. Eng. J.* **1980**, *20*, 391.
(3) Brauer, E. B. Ph.D. Dissertation, The University of Texas, Austin, TX, 1961.
(4) Simon, R.; Rosman, A.; Zana, E. *Soc. Pet. Eng. J.* **1978**, *18*, 20.
(5) Jennings, H. Y. *Rev. Sci. Instrum.* **1968**, *39*, 386.
(6) Fordham, S. *Proc. R. Soc. London., Ser. A* **1948**, *194*, 1.
(7) Sage, B. H.; Lacey, W. N. "Thermodynamic Properties of the Lighter Paraffin Hydrocarbons and Nitrogen"; Monograph on API Research Project 37; American Petroleum Institute: New York, 1950.
(8) Stegemeier, G. L. Ph.D. Dissertation, University of Texas, Austin, TX, 1959.
(9) Olds, R. H.; Reamer, H. H.; Sage, B. H.; Lacey, W. N. *Ind. Eng. Chem.* **1949**, *41*, 475.
(10) Brauer, E. B.; Hough, E. W. *Prod. Mon.* **1965**, *29*, 13.
(11) Levelt Sengers, J. M. H.; Greer, W. L.; Sengers, J. V. *J. Phys. Chem. Ref. Data* **1976**, *5*, 1.
(12) Le Guillou, J. C.; Zinn-Justin, J. *Phys. Rev. B* **1980**, *21*, 3976.

Received for review July 30, 1984. Accepted May 24, 1985. Financial support for this work was furnished by the following organizations: Amoco Production Research Co., ARCO Oil and Gas Co., Chevron Oil Field Research Co., Cities Service Co., Exxon Production Research Co., Marathon Oil Co., Mobil Research and Development Corp., Shell Development Co., Sun Exploration and Production Co., and Texaco, Inc.

Enthalpies of Mixing of Tetrahydrofuran + γ-Butyrolactone and Water + γ-Butyrolactone Systems at 299.15 K

D. H. S. Ramkumar and A. P. Kudchadker*

Department of Chemical Engineering, Indian Institute of Technology, Bombay, India

D. D. Deshpande†

Department of Chemistry, Indian Institute of Technology, Bombay–400 076, India

Enthalpies of mixing have been reported for the systems tetrahydrofuran (THF) + γ-butyrolactone and water + γ-butyrolactone at 299.15 K and 1.013 bar. Data have been fitted to the Redlich–Kister type equation.

Introduction

Enthalpies of mixing ΔH^m are necessary for the treatment of isobaric vapor–liquid equilibrium data as well as in distillation column design calculations. In our present thermodynamic studies of tetrahydrofuran (THF) + water + γ-butyrolactone system, ΔH^m data are available only for the tetrahydrofuran (THF) + water system (*1–3*). Hence, it was decided to measure ΔH^m data for the binary mixtures (i) THF + γ-butyrolactone and (ii) water + γ-butyrolactone.

Experimental Section

Materials. Tetrahydrofuran (THF), supplied by Sarabhai Chemicals, India, was found to be 99.68 mol % pure by GC on a column packed with Carbowax 20M using thermal conductivity detector.

Double distilled deionized water with 2 μmho cm^{-1} electrical conductivity was used for the measurements.

† Present address: Polymer Lab, Department of Chemistry, McGill University, Montreal, Canada.

Table I. Enthalpies of Mixing, ΔH^m, of the THF + Water System at 299.15 K

	ΔH^m/J mol^{-1}		
	at 299.15 K,	at 298.15 K	
x_{THF}	present values[a]	ref 1[b]	ref 2[c]
0.0476	−504	−534[d]	−527[e]
0.1572	−743	−730	−740
0.2572	−625	−650	−657
0.5123	−215	−200	−213

[a] ±14 J mol^{-1}. [b] ±4 to ±8 J mol^{-1}. [c] ±8 J mol^{-1}. [d] At x_{THF} = 0.049. [e] At x_{THF} = 0.05.

Table II. Enthalpies of Mixing ΔH^m of the Two Binaries at 299.15 K

x	ΔH^m/J mol^{-1}	x	ΔH^m/J mol^{-1}
x(Water) + (1 − x)(γ-Butyrolactone)		x(THF) + (1 − x)(γ-Butyrolactone)	
0.1237	237	0.0957	48
0.1971	619	0.1977	91
0.3909	915	0.2944	138
0.4934	774	0.3926	203
0.7163	96	0.4891	197
0.8524	14	0.5953	113
0.8932	5	0.6953	98
0.9645	−23	0.9084	46
0.9703	−26		

Fluka AG Switzerland make γ-butyrolactone of 99.02 mol % purity, as determined chromatographically on a column packed with 12% EGS (ethylene glycol succinate) on Anakrom using thermal conductivity detector, was used.

0021-9568/85/1730-0491$01.50/0